RSC Advances

PAPER

View Article Online
View Journal | View Issue

Cite this: *RSC Adv.*, 2016, **6**, 37463

One-step facile fabrication of controllable microcone and micromolar silicon arrays with tunable wettability by liquid-assisted femtosecond laser irradiation†

Guoqiang Li,‡[a] Zhen Zhang,‡[a] Peichao Wu,[a] Sizhu Wu,[b] Yanlei Hu,[a] Wulin Zhu,[a] Jiawen Li,*[a] Dong Wu,*[a] Xiaohong Li[c] and Jiaru Chu[a]

Received 16th March 2016
Accepted 31st March 2016

DOI: 10.1039/c6ra06949e

www.rsc.org/advances

Micro/nanostructured silicon surfaces are attracting more and more research attention because of the wide range of applications in optoelectronic devices, microelectronics, microfluidics, and biomedical devices. Despite numerous efforts for fabricating a variety of micro/nanostructures, a one-step, facile and effective method for preparing diverse, three-dimensional micro/nanostructures is still desired. In this paper, a new approach based on liquid (ethanol and sucrose solution) assisted femtosecond laser irradiation on silicon substrates was proposed for the preparation of controllable microcones and micromolars arrays. Their height can be controlled from 3.3 to 17.6 μm for microcones and 5.9∼33.7 μm for micromolars by adjusting the pulse energy. The processed surfaces are superhydrophilic (25.05∼2.46°), superoleophilic (7.22∼0°), and underwater superoleophobic (124.9∼169.2°). The surfaces further demonstrate many distinct functions such as fog collecting and volatilizing, droplet storage and transportation, and liquid directional transfer. Our proposed method features rapidness, simplicity and easiness of large-area fabrication, which may find enormous potential applications in many fields such as microfluidic devices, fluid microreactors, biomedicine, and chemical–biological sensors.

1. Introduction

Fabrication of a high density array of high-aspect-ratio silicon micro/nanostructures has attracted considerable attention as of late due to their broad applications in the fields of optical devices,[1] solar cells,[2] sensors,[3] microfluidics[4] and biomedical devices.[5] Standard and conventional electron beam lithography[6,7] and focused ion beam lithography[8] are usually involved in the fabrication of silicon micro/nanostructures with high resolution, however, these technologies have the disadvantages of low throughput or expensive setup. Nanoimprint lithography[9–11] have the advantages of high speed, low cost, large pattern area, and high pattern density, but it still needs a master mold manufactured by means of e-beam or X-ray lithography. Self-organized electrochemical processing[12,13] is an attractive method for fabricating silicon micro/nanostructures as it offers several advantages including a large area and fast speed. However, the preparation is limited by the not as well defined shapes and the sizes of the micro/nanostructures. Especially, these methods need complex multistep manipulation or some special chemical materials.

Recently, laser processing has emerged as an innovative method which is one-step, fast and maskless way to prepare special nanoparticles and surface micro/nanostructures to overcome the disadvantages of traditional methods.[14–34] For instance, E. Fadeeva[31] and A. A. Ionin's[32] have reported the fabrication of self-organized conical pillars on the titanium surface by femtosecond laser ablation in air. In addition to the metal, many scientists have also conducted femtosecond laser fabrication semiconductor materials, such as silicon, which is broadly used in biomedicine, optoelectronics, micro-electronics and other fields.[23–27,29,30] Many groups, such as E. Mazur,[25–27] E. Stratakis[28] have prepared controllable sharp spikes by SF_6, Cl_2 or H_2S assisted femtosecond laser irradiation. In terms of the formation of microstructures, these reaction gases assisted processing is effective, fast compared in air, N_2, and even vacuum.[25–28] However, SF_6 and Cl_2 are hazardous gas, which can cause severe harm to the operators and environments.[25–28] Moreover, during the process of these kind of dry treating,

[a]*CAS Key Laboratory of Mechanical Behavior and Design of Materials, Department of Precision Machinery and Precision Instrumentation, University of Science and Technology of China, Hefei, Anhui, 230026, China. E-mail: dongwu@ustc.edu.cn; jwl@ustc.edu.cn*

[b]*School of Instrument Science and Opto-electronics Engineering, Hefei University of Technology, Hefei, Anhui, 230009, China*

[c]*Joint Laboratory for Extreme Conditions Matter Properties, School of Science, Southwest University of Science and Technology, Mianyang, Sichuan, 621010, China*

† Electronic supplementary information (ESI) available. See DOI: 10.1039/c6ra06949e

‡ G. Q. Li and Z. Zhang contributed equally to this work.

a high-precision but costly vacuum chamber is usually required to pump the reactant gas.[25–28] In recent years, many groups have concentrated on the liquid-assisted processing by femtosecond laser pulses.[14–20,23,24,33,34] S. Barcikowski,[14,15] M. Meunier,[16,17] V. Amendola,[18,19] *et al.*, have prepared controllable Au nanoparticles in aqueous solutions or organic solvents assisted laser irradiation. S. Bashir[21] has investigated the formation of desired morphology and chemical composition on Ti and zirconium surfaces in ethanol. S. Hamad[22] has fabricated silicon nanoparticles and self-organized high spatial frequency laser induced periodic surface structures (HSFL) by femtosecond laser ablation Si in acetone. E. Mazur[23,24] has reported the formation of 200 nm wide silicon spikes, high-density regular arrays of nanometer-scale silicon rods in water. All these works declare that femtosecond laser irradiation in liquid environments are simple and fast methods in creating micro/nanostructured surfaces. Although many works are involved with the femtosecond laser ablation silicon in ethanol, the products are mainly nanoparticles and few refers to micro/nanostructures.[35] Additionally, as a common high viscosity solution, sucrose solvent has never been reported as assisted liquid environment in laser micro/nanofabrication.

In this work, we use low-boiling, low viscosity ethanol, and for the first time employ the high boiling point and high-viscosity sucrose as liquid environment for femtosecond laser irradiation on silicon. The microcone and micromolar arrays were successfully prepared in ethanol and sucrose, respectively. It is indicated that the heights are tunable by simply controlling the laser pulse energy. Furthermore, these processed surfaces exhibit multiple functions, such as collecting fog, liquid storage, microdroplet manipulation and directional transfer, which can be used in microfluidic devices, fluid microreactors, biomedicine, biomedical scaffolds, and chemical–biological sensors.[29,30,33,34]

2. Experimental section

2.1 Materials

In our experiments, single crystal p-type silicon (110) with dimension of $0.5 \times 20 \times 20$ mm^3 and $0.5 \times 20 \times 40$ mm^3 were purchased from New Metal Material Tech. Co., Ltd, Beijing, China. The oil used to detect the contact/sliding angles is 1,2-dichloroethane ($C_2H_4Cl_2$). The assisted solvents are ethanol (purity of 99.3%) and sucrose which is prepared by dissolving 50 g sucrose in 50 g distilled water.

2.2 Laser treating silicon surface

The details of the experimental setup and schematic fabrication process are shown in Fig. 1(a). A regenerative amplified Ti:sapphire fs laser system (Legend Elite-1K-HE, Coherent, pulse duration of 104 fs, center wavelength of 800 nm, repetition rate of 1 kHz) is employed for the irradiation experiment. To induce micro/nanostructures with different heights at large area, the pulse energies of the incident laser are set from 0.05 to 0.25 mJ, and the scanning speed is constant (1 mm s^{-1}). The step sizes between the adjacent scanning lines are 20, 35, and 50 μm, respectively. For liquid experiments, the silicon sheet was stuck to the bottom of a 20 ml glass container. When the glass container was filled up with ethanol or sucrose, the height of the liquid layer above the sample surface was about 12 mm. In this experiment, the focusing condition is an vitally important parameter, which can greatly influence the energy distribution and morphology of the formed micro/nanostructures. The glass container (vessel) containing the sample was mounted on a computer controlled *XYZ* translation stage for precisely positioning of the area to be machined. Considering the different focal conditions in air and liquids due to refractive effects, we adjusted the position of focal plane by moving the sample along the optical axis (*Z* direction) in order to obtain the same focal positions. During the adjustment process, a CCD camera was used for *in situ* observation. The detailed description of the focusing conditions is shown in the ESI [Fig. S1–S3†].

2.3 Characterization of structured silicon surface

The structural properties of the as-prepared samples are investigated by scanning electron microscope (SEM, JSM-6700F, JEOL, Tokyo, Japan) and optical microscope (Nikon, Japan). The contact angles of 5 μl water or oil droplet, and the sliding angles of the oil droplet underwater are measured by a contact-angle system (CA100D, Innuo, China). The photographs and the videos are taken by a digital camera (Sony, Japan).

3. Results and discussion

3.1 Formation of microcone and micromolar arrays in ethanol and sucrose solutions

The ethanol has the high density of 99.3%, low boiling point of 78.4 °C and low viscosity. On the contrary, the sucrose solution has the high boiling point (higher than 100 °C) and high viscosity. The physical properties for the two solutions are very different. So, the laser interaction mechanism between silicon and different solvent may be different. Moreover, in our previous works, we have reported the one-step assembly of 3-dimensional porous metal micro/nanocages by ethanol-assisted femtosecond laser irradiation for enhanced antireflection and hydrophobicity,[33] and the preparation of underwater superoleophobic microcones arrays by sucrose solution assisted femtosecond laser irradiation.[34] In this work, we also used ethanol and sucrose solution as liquid environment to assist the femtosecond laser fabrication on silicon surfaces.

SEM images in Fig. 1(b) indicate the silicon surface micro/nanostructures prepared in air at pulse energy of 0.06 mJ, scanning speed of 1 mm s^{-1}, and scanning space of 50 μm. It is observed that the structures are mainly nanoparticles covered cloud-structures with various sizes, displaying random, which can be attributed to silicon vapor cloud formed on and above the surface during its heating by the laser radiation, and the redeposition of the multiscale nanoparticles produced by the laser impact effect.[36]

Fig. 1(c) exhibits that the formation of the microcones with the ethanol-assisted fs laser irradiation. It is indicated that the

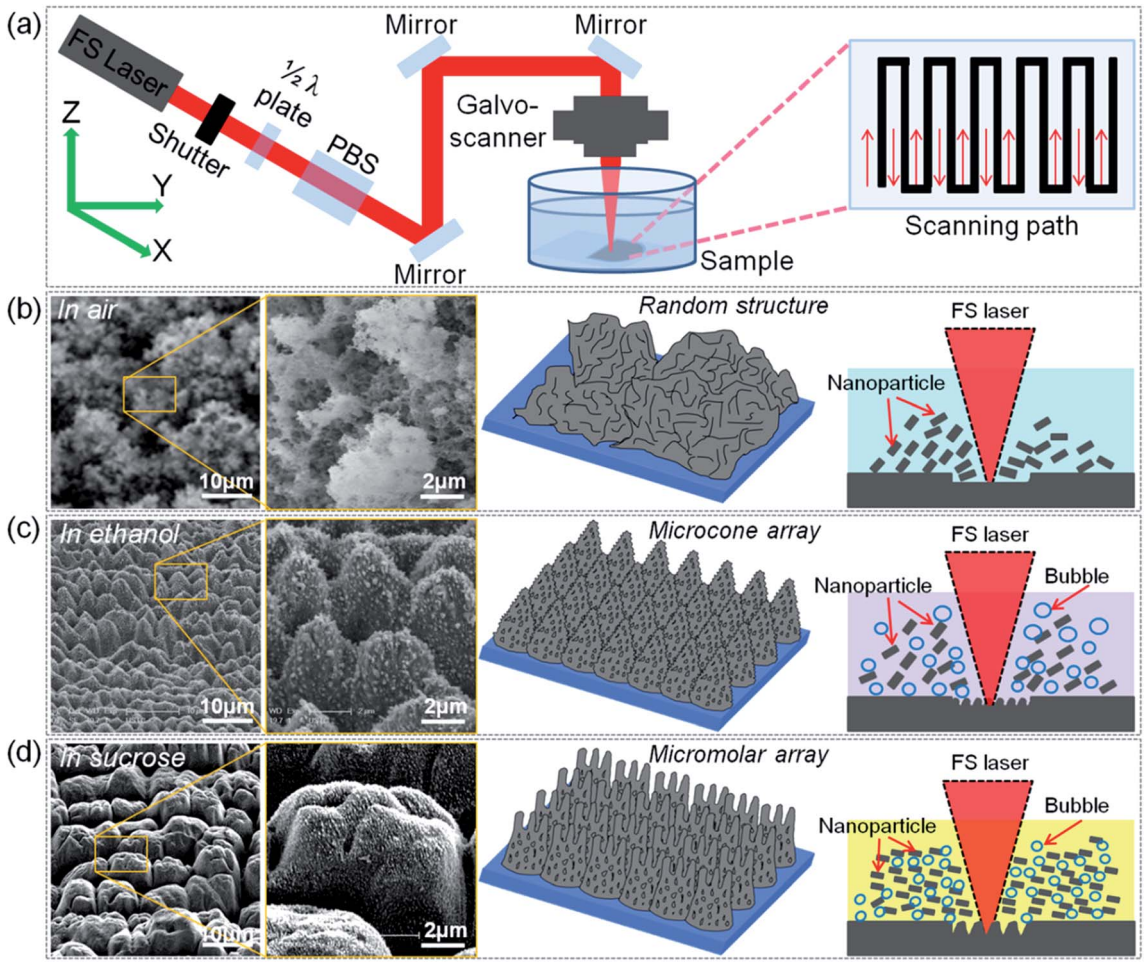

Fig. 1 The preparation of microcones and micromolars with ethanol and sucrose solution assisted fs laser irradiation at pulse energy of 0.06 mJ. (a) Schematic representation of the experimental setup. (b) Random structures in air under the same laser parameters. The structures consisted of cotton-like structures covered with debris of silicon. (c) Microcones arrays with ethanol assisted fs laser irradiation. The microcones height is about 3.3 μm. During the experiment, few but large bubbles were produced at the ethanol/silicon interface, and nanoparticles were also formed. (d) Micromolars arrays with sucrose solution assisted fs laser irradiation. The morphology of the microstuctures like mammal molars and the height is about 5.9 μm. A lot of tiny bubbles and nanoparticles were generated during the experiment.

microcones are regularly distributed and the average height is about 3.3 μm. Different from the micro/nanostructures prepared in ethanol, the formed micro/nanostructures in sucrose solution can be described as micromolars [Fig. 1(d)] with the height of 5.9 μm. It is seen that the microcones and micromolars are distributed into arrays.

The mechanism for the formation of such structures can be ascribed to the high temperature of plasma excited at the silicon/liquid interface and the capillary wave excited in the molten silicon thin layer during the localized cooling process.[23,37] By contrast, it is observed that during the machining process, there were more and smaller bubbles produced than that in ethanol. In addition, the processing in sucrose solution is more peaceful. The differences of density, viscosity as well as boiling point of the ethanol and sucrose also have great influence in inducing the diverse microstructures on silicon surface. Therefore, the ambient conditions are critical for the formation of different micro/nanostructures.

3.2 Precisely controlling the growth of the microcones and micromolars arrays by the laser pulse energy

From the aspect of practical application, it is acceptable to fabricate controllable structures *via* a simple parameter. Based on the experimental observation, the growth of both the microcones and micromolars arrays can be effectively controlled by adjusting the laser pulse energy. In order to illustrate this controllability, a series of pulse energy ranged from 0.05 to 0.25 mJ is chosen to do the irradiation experiments. With the increasing pulse energy, the laser-induced plasma is further expanded to produce a stronger shock wave, higher temperature and higher pressure at the interface, so higher and larger microcones and micromolars are produced. For example, when the pulse energy is increased from 0.05 to 0.25 mJ, the height can be increased from 3.3 to 17.6 μm for microcones [Fig. 2(a)] and from 5.9 to 33.7 μm for micromolars [Fig. 2(b)], respectively [ESI, Fig. S4†]. Additionally, it can be seen that the grooves with the adjacent spaces of 50 μm are also

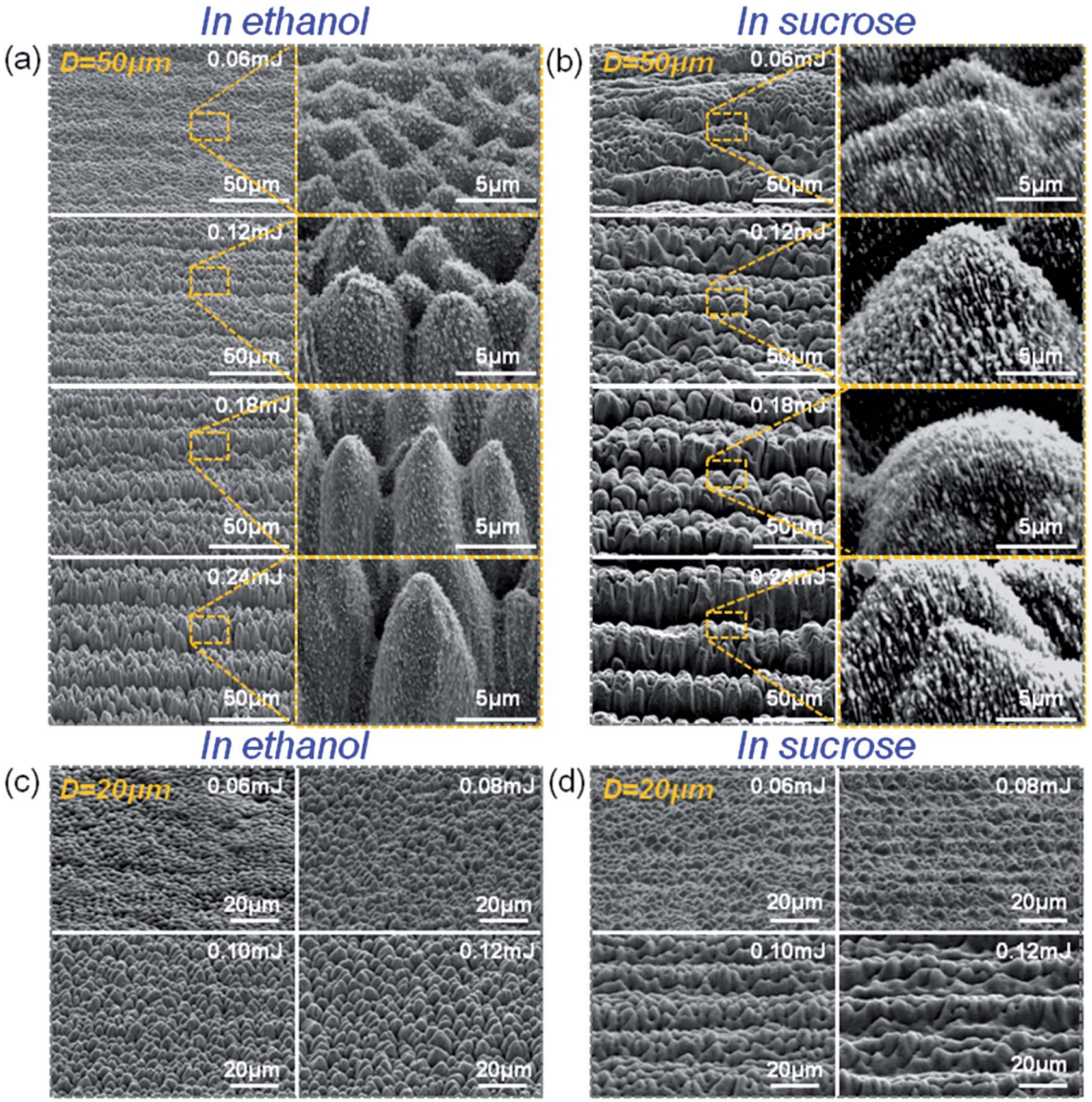

Fig. 2 Precisely controlling the growth of the microcone and micromolar arrays by adjusting the laser pulse energy. (a) 45° tilted SEM images of the silicon surfaces by fs laser irradiation in ethanol with $D = 50$ μm at pulse energy from 0.06 to 0.24 mJ. The microcones are uniformly distributed and the height is increased from 3.3 to 17.6 μm with the increasing pulse energy. (b) 45° tilted SEM images of the micromolars fabricated in sucrose solution. The corresponding height is ranged from 5.9 to 33.7 μm. (c) and (d) SEM images of the microcones and micromolars prepared at $D = 20$ μm, pulse energy of 0.06∼0.12 mJ, and the energy interval is 0.02 mJ. Under this processing condition, all the microcones are still uniformly distributed on the whole processed surface, however for micromolars there are always groove caused by the scanning lines.

formed between the micro/nanostructures, with the period equal to the direction translation step due to the scanning of the laser beam.

In order to further investigate the evolution of the microcones and micromolars, and the formation of the grooves, we conduct another experiment with the pulse energy ranged from 0.06 to 0.12 mJ, and the scanning spaces of 20 μm [Fig. 2(c) and (d)]. In Fig. 2(c), at pulse energy of 0.06 mJ, it is seen that small microcones with height of 3∼3.5 μm are partly generated on the processed area. With the increasing pulse energy, the microcones gradually grow larger, and the height is 4.1∼5.2 μm at 0.08 mJ, 5.5∼6.3 μm at 0.10 mJ, and 6.5∼7.1 μm at 0.12 mJ. In addition, the distributions become more uniform with the increasing pulse energy. The SEM images in Fig. 2(d) indicate that the micromolars also grow as a function of the pulse energy, and the height can reach about 9.4 μm at 0.12 mJ. By comparing the results in Fig. 2(c) and (d), it is found that the micromolars are always larger than the microcones produced at the same parameter. Another distinct difference is that the grooves can be always formed under the sucrose solution assisted fs laser irradiation. The generation mechanism for these differences can be attributed to the different boiling points, viscosity, and refractive index of ethanol and sucrose solution. E. Mazur[23] has reported the

formation silicon spikes by liquid (water) assisted femtosecond laser pulses irradiation, however, the size of the structures are 200 nm, which are obviously smaller than laser wavelength of 800 nm. F. Chen[29,30] *et al.* has presented an effective method of producing hierarchical conical spike structures femtosecond laser irradiation in air through a line-by-line and serial scanning process. It is indicated the formation of the conical spikes can be attributed to the femtosecond laser holing, and the period of the structures is equal to the spaces of the adjacent pulse, which is different from our strategy. This experiment demonstrates that a simple and flexible method have been proposed to fabricate controllable microcones and micromolars on silicon surfaces.

3.3 The wettability of the microcones and micromolars arrays

3.3.1 The superhydrophilicity/superoleophilicity. E. Mazur[27] has already investigated the wettability of the structured silicon surface, however, they focused on the superhydrophobicity which is obtained by modified the surface with a layer of fluoroalkylsilane molecules. Here, different from the literature,[27,29,30] we mainly studied the superhydrophilicity/superoleophilicity of the micro/nanostructured surface. In our experiment, the water and oil contact angle of the flat silicon surface is about 36.2° and 24.7° in air, demonstrating intrinsically weak hydrophilicity and oleophilicity, respectively [ESI, Fig. S2†]. It is reported that the hydrophilic/oleophilic flat surface can be tuned to be more hydrophilic/superhydrophilic, or more oleophilic/superoleophilic one by introducing the rough hierarchical micro/nanostructures.[38] Fig. 3(a) shows the contact angles (CA) as functions of the pulse energy for inducing microcones and micromolars with different roughness. It can be seen that the water CA decreased with the increasing pulse energy, from 24.5° to 3.2° for microcones, 12.3° to 2.6° for micromolars. Due to the hydrophilicity, the water can completely contact the rough surface, as shown in the schematic diagram of Fig. 3(a), forming the Wenzel contact. The contact model (Wenzel model)[39,40] can be described as follows

$$\cos \theta'_{WA} = R \cos \theta_{WA} \quad (1)$$

where θ'_{WA} and θ_{WA} are the water CA on the structured silicon surface and flat one [ESI, Fig. S5†], respectively. R is the roughness factor,[41] defined as the ratio of the actual apparent surface areas of the microcones and micromolars to their geometric projected areas. In our case, the value of R is greater than 1,[33,34] and it is increased with the pulse energy. According to Wenzel's model, the hydrophilic surfaces will be more hydrophilic with the increase of roughness. The CA measurement also shows that the structured silicon surfaces fabricated in sucrose solution are more hydrophilic than that in ethanol. Meanwhile, we find that scanning space also influence the water CA to a small degree, namely the water droplet has smaller CA at smaller scanning space. As seen from Fig. 3(b), all the oil CAs on the structured silicon surface are less than 10° due to the lower surface tension, showing superoleophilicity. Similar to the case in Fig. 3(a), the oil contact angle is decreased with the increasing pulse energy and the decreasing scanning space. It's worth mentioning that the water droplet can quickly spread on the micromolars induced at pulse energy above 0.18 mJ in sucrose solution, and finally the contact angle nearly reaches 0, showing extremely superhydrophilicity.

The properties of superhydrophilicity and superoleophilicity are crucial for preparing multi-functionalized surfaces. To this end, a fog collector constituted by three concentric rings spaced by unprocessed areas [Fig. 3(c)] is designed and placed into the artificial fog flow condition to reveal the enhanced fog harvesting. As time prolonged, the micro-droplets from fog are gathered to gradually form larger droplets, randomly distributed on the unprocessed locations. On the contrary, the fog droplet was prior to condense on the processed areas, and then fog water gradually coalesced and covered the concentric rings driven by the wettability difference during the fogging process. The continually collected fog water completely covered the three rings in the end, forming continuous waters. The volatilization behavior of the water droplets, which is an inverse process of the fog collection process, was also investigated [Fig. 3(d)]. It is observed that the tiny water drops on the unprocessed areas is preferentially volatilized, while the water on the processed ones can keep the morphology primly. This investigation indicates that our fog collector can act as a potential fog harvesting apparatus with an enhanced efficiency, which may find applications at the arid regions with freshwater scarcity. Due to the superhydrophilicity and superoleophilicity, the as-prepared silicon surfaces can be used for liquid storage. As shown in Fig. 3(e), oil, red ink and milk can be fixed at the processed three circular areas with 6 mm diameter, orderly. None of the droplets overflow from the designated circular regions, displaying ultrahigh adhesion.

3.3.2 The underwater superoleophobicity and the oil droplet manipulation. When the hydrophilic silicon surface is immersed in water, water molecules can be trapped in the formed micro/nanostructures, developing a composite water/solid interface. For the incompatibility, the trapped water acts as an insulation layer to prevent the oil droplet from permeating into the micro/nanostructures.[29,38] In this case, the oil droplet can only contact the top of the induced micro/nanostructures, hence the processed silicon surface forms an oleophobic and even superoleophobic interface. Fig. 4(a) and (b) indicate the oil contact angles for microcones and micromolars as functions of pulse energy, respectively. It is easy to see that the oil contact angles are increased with the increasing pulse energy, and also they possesses a larger contact angle at smaller scanning space. By comparison, it is found that the micromolars endow the oil droplet with larger contact angle than the microcones. Furthermore, the state of the oil droplet can be described by the Cassie model[40–42] and the contact angle can be expressed as

$$\cos \theta'_{OA} = f \cos \theta_{OA} + f - 1 \quad (2)$$

where θ'_{OA} and θ_{OA} are the oil CA on the structured and flat silicon surfaces, respectively [ESI, Fig. S5†]. f is the area fraction defined as the ratio of the actual contact area possessed by the oil droplet to the whole microstructure area. Although the

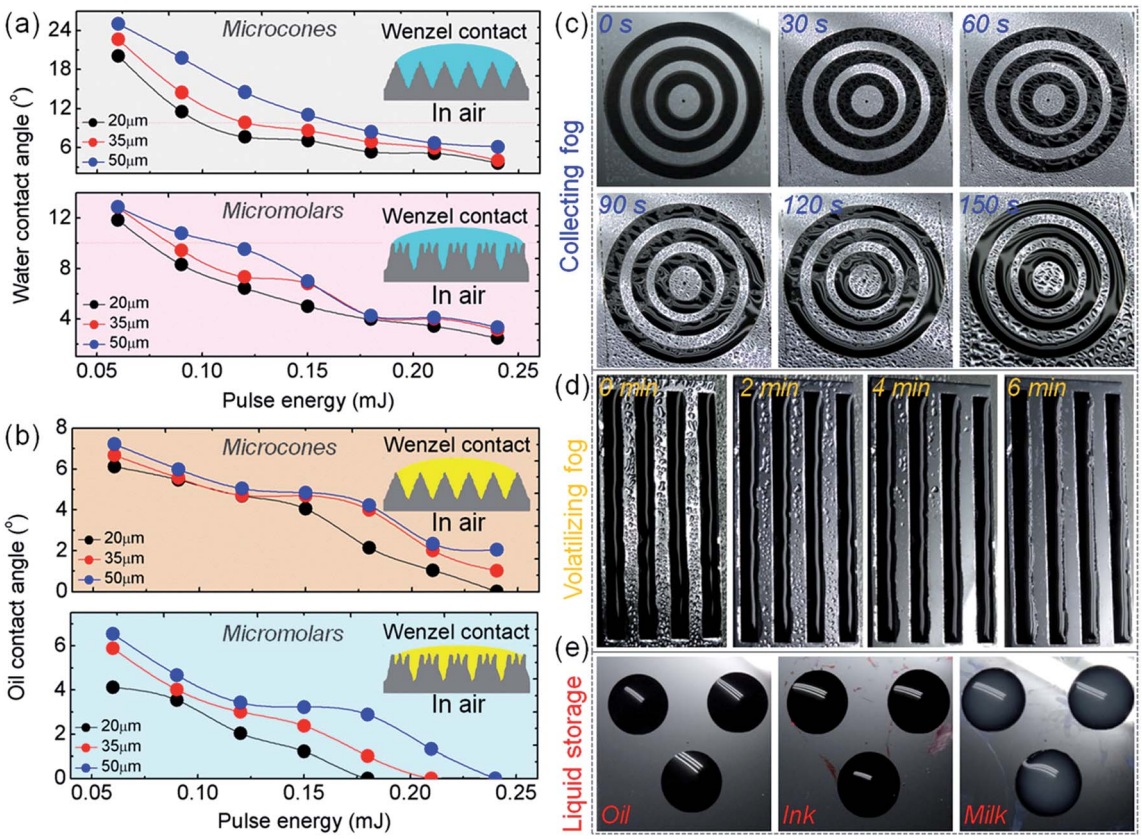

Fig. 3 The superhydrophilicity/superoleophilicity of the microcones and micromolars. (a) The water contact angle of microcones and micromolars. All contact angles decreased with the increasing pulse energy. (b) The oil contact angles of microcones and micromolars. The processed silicon surfaces are superoleophilic. The insert images in (a) and (b) were the illustration of the Wenzel contact model. (c) Sequential optical images of fog collection on microcones-constituted three concentric rings. (d) The volatilization process of the water collected by four 4 cm long lines consisting of micromolars arrays. Both the start time was set as 0 for (c) and (d). (e) The static storage for oil, red ink, and milk. Due to the superhydrophilicity and superoleophilicity, the liquid can be firmly fixed at the processed areas.

exact value of f is not readily available, it can be theoretically deduced from eqn (2), and the calculated results are shown in Fig. 4(c). Obviously, the value of f is decreased with the increasing pulse energy and decreasing scanning space. In addition, it is observed from Fig. 4(a) and (b) that some measured contact angles are below 150°. In this case, the oil droplets are in metastable Wenzel/Cassie hybrid states,[43,44] as shown in the schematic diagram of Fig. 4(d_1) and (d_3). Conversely, when the contact angle is larger than 150°, the contact is the Cassie model, which represents a non-wet-contact mode. The oil contacts the upper end of the micro-structures, leaving the lower end immersed in water [Fig. 4(d_2) and (d_4)]. Especially, the minimum values for f are 0.206 and 0.081 for microcones and micromolars, endowing the structured surface with oil CA of 157.76° and 169.21°. The oil sliding behaviors are also studied [Fig. 4(e) and (f)]. Similar to the case discussed above, the sliding angles are also decreased with the increasing pulse energy and decreased scanning space. The microcones and micromolars can modulate the oil sliding angle from 0.91° to 12.88°, and 0.52° to 9.14°, respectively. Generally, the small sliding angle signifies low adhesion.[45,46]

The modification of the underwater wettability plays an important role in the oil manipulation. Fig. 4(g) and (h) indicate the controlling of the moving behavior of the oil droplet. By utilizing the adhesion contrast between the treated and untreated area, the oil droplet can move along the setting path without loss *via* slightly tilting the sample [ESI, Fig. S6†]. In addition, the structured surfaces with controllable adhesion have important potential application in the transfer of oil droplets. Fig. 4(i) shows an example of transferring a 5 μl oil droplet from the low adhesive A surface to the high adhesive C surface *via* using medium adhesive B surface as a "mechanical hand" [ESI†].[47,48]

3.3.3 The anisotropic wetting and sliding behavior. In the previous discussion, the scanning space (D) was set as 20, 35, and 50 μm, which can match up with the size of focused laser beam, therefore, there is hardly any untreated space between the scanning lines, making the induced microstructures overlap with each other. In this case, the wetting and sliding of the oil in water are isotropic. When increasing the scanning space, blank area appears and gradually grows wider as shown in Fig. 5(a) and (b), which are prepared at pulse energy of 0.25 mJ. By contrasting the preparation in ethanol and sucrose solution, it

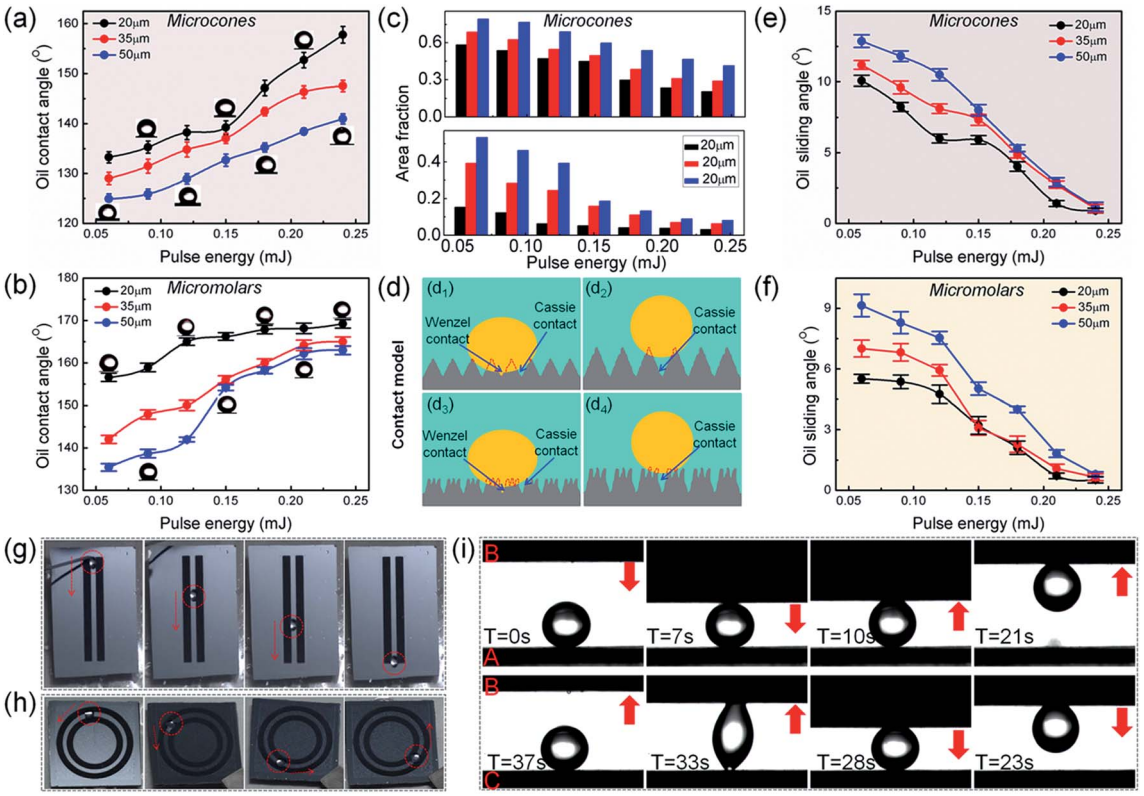

Fig. 4 The underwater superoleophobicity and the oil droplet manipulation. (a) and (b) show that the microcones and micromolars are underwater superoleophobic and the oil contact angles increased with the increasing pulse energy. (c) The calculated area fractions defined as the ratio of actual contact area by the oil droplet to the whole area of the microstructures. It is demonstrated that the area fractions decreased with the increasing pulse energy. (d) The detailed contact model for underwater oil. When the contact angle is smaller, the contact model is metastable Wenzel/Cassie hybrid states. However, if the contact angle is larger, the contact model is Cassie state. (e) and (f) are the oil sliding angles on microcones and micromolars as functions of pulse energy. (g) and (h) The directional transport of oil along the set path. (i) Process of transferring oil droplet from the A surface to C surface *via* B surface. Utilizing the differences of adhesive force, the structured surfaces can be used as "mechanical hand" to transfer the oil droplet from lower adhesive surface to higher one.

is indicated that laser can scan the silicon surface to form the wider scanning lines with the assistance of sucrose solution than ethanol [ESI, Fig. S7†]. The increase of the scanning space results in the difference between the contact angles measured parallel or perpendicular to the scanning lines. Fig. 5(c) and (d) reveal the shapes of a 5 μl oil droplet on the treated silicon surface with D of 80 and 200 μm, along the directions perpendicular and parallel the scanning lines, respectively. Seen from Fig. 5(c) for microcones with $D = 80$ μm, the values for $CA_{\perp}$ and $CA_{\parallel}$ are 153.92° and 151.83°, declaring a small degree of wetting anisotropy for the two directions. However, for $D = 200$ μm, the measured $CA_{\perp}$ and $CA_{\parallel}$ are 138.08° and 124.36°, hence the difference of the CA values for the two directions is 13.72°. Similarly, for micromolars, at $D = 80$ μm, the $CA_{\perp}$ and $CA_{\parallel}$ are 166.29° and 162.72°, and at $D = 200$ μm the values are 143.81° and 131.52°, respectively [Fig. 5(d)]. We also systematically investigated the influence of D on the values for CAs of oil in the perpendicular and parallel directions on both microcones and micromolars [Fig. 5(e)]. It can be seen that although both the $CA_{\perp}$ and $CA_{\parallel}$ are decreased with the increasing D, $CA_{\perp}$ is consistently larger than $CA_{\parallel}$. Furthermore, $CA_{\parallel}$ is initially approximate to $CA_{\perp}$, however, with D increasing, the $CA_{\parallel}$ is decreased much faster for the more and more obvious anisotropic structure.

To investigate the influence of D on the anisotropic sliding of the oil droplets, the SAs perpendicular and parallel to the scanning lines [Fig. 5(f)] were measured. Fig. 5(g) and (h) indicate the snapshots of an oil droplet rolling on tilted microcones and micromolars silicon surface with D of 80 and 200 μm, respectively. At D of 80 μm, the $SA_{\perp}$ and $SA_{\parallel}$ are 1.13° and 2.87° for microcones, 0.81° and 0.84° for micromolars, showing small sliding anisotropy. However at D of 200 μm, the measured $SA_{\perp}$ and $SA_{\parallel}$ are 48.24° and 58.79° for microcones, inducing sliding anisotropy is 10.55°. While for micromolars, the $SA_{\perp}$ is 21.45° and $SA_{\parallel}$ is 44.29°, which indicates that the sliding anisotropy reaches 22.84°. The relationship between the anisotropic sliding and D for the microcones and micromolar was systematically studied [Fig. 5(i)]. From Fig. 5(i), it is observed that the SAs in the parallel direction were always smaller than those in the perpendicular direction. This anisotropic sliding is caused by the different three-phase contact line (TCL).[47–49] By comparison, the discontinuous and long TCL perpendicular to the scanning lines can give rise to more pronounced hysteresis effects than the continuous short ones along the parallel direction.

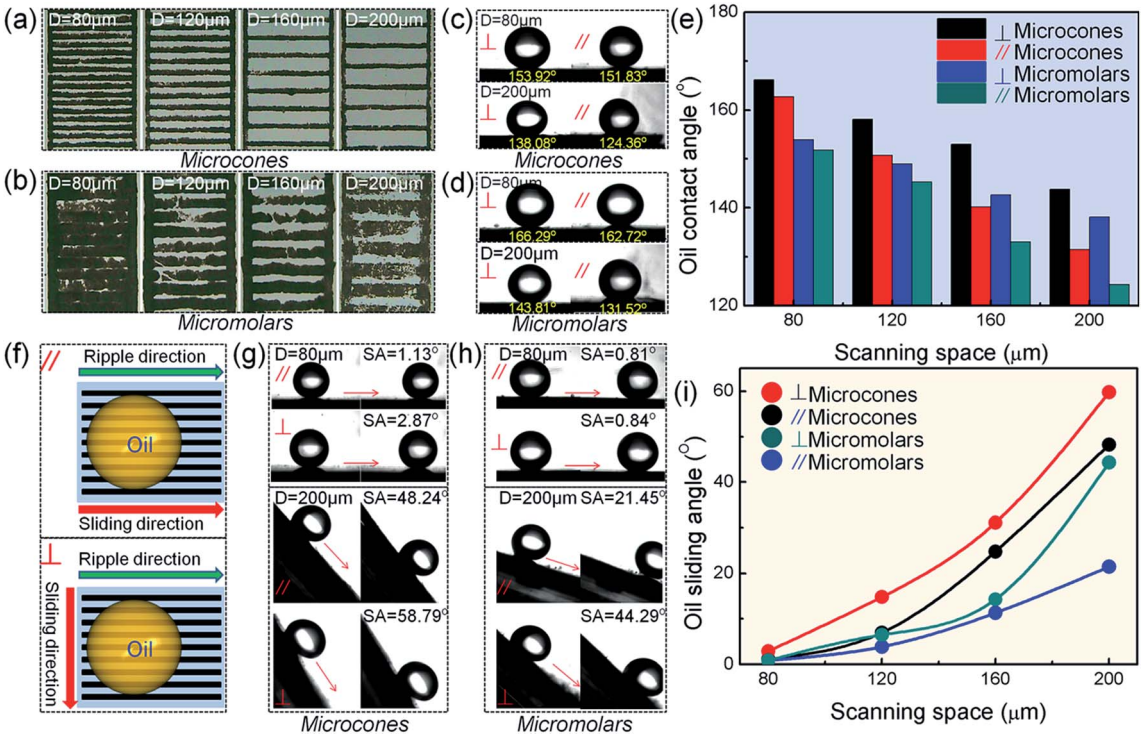

Fig. 5 The anisotropic wetting and sliding behavior. (a) and (b) are the optical microscope images of the silicon surfaces prepared by ethanol and sucrose solution assisted fs laser irradiation under pulse energy of 0.25 mJ and scanning space of 80, 120, 160, and 200 μm, respectively. (c) and (d) The optical images of the anisotropic contact state of 5 μl oil which were measured perpendicular and parallel to the scanning lines composed by microcones and micromolars, respectively. (e) The statistical results of the oil anisotropic contact angles with the increasing scanning spaces. (f) The schematic illustration of oil droplet slides perpendicular and parallel to the scanning lines. (g) and (h) The snapshots of oil droplet rolling on the microcones and micromolars surfaces with scanning spaces of 80 and 200 μm, along the parallel and perpendicular directions, respectively. (i) The oil anisotropic sliding angles as a function of the scanning space.

4. Conclusion

In this work, we have developed a facile approach of one-step assembling microcones and micromolars on silicon surfaces by ethanol and sucrose solution-assisted fs laser irradiation. By simply changing the solutions and adjusting the pulse energy, the height of the microcones and micromolars can be arbitrarily controlled, which endow the silicon surfaces with tunable superhydrophilic, superoleophilic, and underwater superoleophobic properties. In addition, these micro/nanostructured surfaces also show many useful multifunctions, such as fog collecting and volatilizing, liquid storage and transportation, and directional transfer. The unique wetting properties of the structured silicon surfaces by our proposed method open new applications in fields of microfluidic devices, fluid microreactors, biomedicine, and chemical–biological sensors.

Acknowledgements

This work is supported by National Natural Science Foundation of China (No. 51275502, 61475149, 51405464, 91223203, and 11204250), Anhui Provincial Natural Science Foundation (No. 1408085ME104), National Basic Research Program of China (No. 2011CB302100), the Fundamental Research Funds for the Central Universities (No. WK2090000006 and WK2090090018) and "Chinese Thousand Young Talents Program".

References

1 A. Liu, R. Jones, L. Liao, D. Samara-Rubio, D. Rubin, O. Cohen, R. Nicolaescu and M. Paniccia, *Nature*, 2004, **427**, 615–618.
2 B. Tian, X. Zheng, T. Kempa, Y. Fang, N. Yu, G. Yu, J. Huang and C. Lieber, *Nature*, 2007, **449**, 885–889.
3 O. H. Elibol, D. Morisette, D. Akin, J. Denton and R. Bashir, *Appl. Phys. Lett.*, 2003, **83**, 4613–4615.
4 G. Whitesides, *Nature*, 2006, **442**, 368–373.
5 D. Kim, J. Ahn, W. Choi, H. Kim, T. Kim, J. Song, Y. Huang, Z. Liu, C. Lu and J. Rogers, *Science*, 2008, **320**, 507–511.
6 W. Chen and H. Ahmed, *Appl. Phys. Lett.*, 1993, **62**, 1499–1501.
7 D. Carr and H. Craighead, *J. Vac. Sci. Technol., B: Microelectron. Nanometer Struct.–Process., Meas., Phenom.*, 1997, **15**, 2760–2763.
8 A. Chelnokov, K. Wang, S. Rowson, P. Garoche and J. Lourtioz, *Appl. Phys. Lett.*, 2000, **77**, 2943–2945.
9 L. Guo, P. Krauss and S. Chou, *Appl. Phys. Lett.*, 1997, **71**, 1881–1883.

10 Z. Yu, H. Gao, W. Wu, H. Ge and S. Chou, *J. Vac. Sci. Technol., B: Microelectron. Nanometer Struct.–Process., Meas., Phenom.*, 2003, **21**, 2874–2877.
11 Q. Zheng, B. Zhou, J. Bai, L. Li, Z. Jin, J. Zhang, J. Li, Y. Liu, W. Cai and X. Zhu, *Adv. Mater.*, 2008, **20**, 1044–1049.
12 J. Schultze and K. Jung, *Electrochim. Acta*, 1995, **40**, 1369–1383.
13 C. Martin, M. Blunt and P. Moriarty, *Nano Lett.*, 2004, **4**, 2389–2392.
14 S. Petersen, A. Barchanski, U. Taylor, S. Klein, D. Rath and S. Barcikowski, *J. Phys. Chem. C*, 2010, **115**, 5152–5159.
15 S. Barcikowski and G. Compagnini, *Phys. Chem. Chem. Phys.*, 2013, **15**, 3022–3026.
16 A. V. Kabashin, M. Meunier, C. Kingston and J. H. T. Luong, *J. Phys. Chem. B*, 2003, **107**, 4527–4531.
17 J. P. Sylvestre, S. Poulin, A. V. Kabashin, E. Sacher, M. Meunier and J. H. T. Luong, *J. Phys. Chem. B*, 2004, **108**, 16864–16869.
18 V. Amendola, S. Polizzi and M. Meneghetti, *J. Phys. Chem. B*, 2006, **110**, 7232–7237.
19 V. Amendola, S. Polizzi and M. Meneghetti, *Langmuir*, 2007, **23**, 6766–6770.
20 C. Albu, A. Dinescu, M. Filipescu, M. Ulmeanu and M. Zamfirescu, *Appl. Surf. Sci.*, 2013, **278**, 347–351.
21 S. Bashir, M. S. Rafique, C. S. Nathala and W. Husinsky, *Appl. Phys. A*, 2014, **114**, 243–251.
22 S. Hamad, G. K. Podagatlapalli, V. S. Vendamani, S. V. S. N. Rao, A. P. Pathak, S. P. Tewari and S. V. Rao, *J. Phys. Chem. C*, 2014, **118**, 7139–7151.
23 M. Y. Shen, C. H. Crouch, J. E. Carey and E. Mazur, *Appl. Phys. Lett.*, 2004, **85**, 5694–5696.
24 M. Y. Shen, J. E. Carey, C. H. Crouch, M. Kandyla, H. A. Stone and E. Mazur, *Nano Lett.*, 2008, **8**, 2087–2091.
25 T. H. Her, R. J. Finlay, C. Wu and E. Mazur, *Appl. Phys. A*, 2000, **70**, 383–385.
26 M. A. Sheehy, L. Winston, J. E. Carey, C. M. Friend and E. Mazur, *Chem. Mater.*, 2005, **17**, 3582–3586.
27 T. Baldacchini, J. E. Carey, M. Zhou and E. Mazur, *Langmuir*, 2006, **22**, 4917–4919.
28 A. Ranella, M. Barberoglou, S. Bakogianni, C. Fotakis and E. Stratakis, *Acta Biomater.*, 2010, **6**, 2711–2720.
29 J. Yong, F. Chen, Q. Yang, D. Zhang, U. Farooq, G. Du and X. Hou, *J. Mater. Chem. A*, 2014, **2**, 8790–8795.
30 J. Yong, Q. Yang, F. Chen, H. Bian, G. Du, U. Farooq and X. Hou, *Adv. Mater. Interfaces*, 2015, **2**, 1400388.
31 E. Fadeeva, V. K. Truong, M. Stiesch, B. N. Chichkov, R. J. Crawford, J. Wang and E. P. Ivanova, *Langmuir*, 2011, **27**, 3012–3019.
32 A. A. Ionin, S. I. Kudryashov, S. V. Makarov, A. A. Rudenko, L. V. Seleznev, D. V. Sinitsyn, E. V. Golosov, Y. R. Kolobov and A. E. Ligachev, *Appl. Phys. A*, 2014, **116**, 1133–1139.
33 G. Li, J. Li, C. Zhang, Y. Hu, X. Li, J. Chu, W. Huang and D. Wu, *ACS Appl. Mater. Interfaces*, 2015, **7**, 383–390.
34 G. Li, Y. Lu, P. Wu, Z. Zhang, J. Li, W. Zhu, Y. Hu, D. Wu and J. Chua, *J. Mater. Chem. A*, 2015, **3**, 18675–18683.
35 P. G. Kuzmin and G. A. Shafeev, *J. Phys. Chem. C*, 2010, **114**, 15266–15273.
36 A. Y. Vorobyev and C. L. Guo, *Appl. Surf. Sci.*, 2011, **257**, 7291–7294.
37 P. G. Kuzmin and G. A. Shafeev, *J. Appl. Phys.*, 2012, **112**, 104314.
38 M. Liu, S. Wang, Z. Wei, Y. Song and L. Jiang, *Adv. Mater.*, 2009, **21**, 665–669.
39 J. Liu, X. Feng, G. Wang and S. Yu, *J. Phys.: Condens. Matter*, 2007, **19**, 356002.
40 Z. Xue, Y. Cao, N. Liu, L. Feng and L. Jiang, *J. Mater. Chem. A*, 2014, **2**, 2445–2460.
41 J. Yong, Q. Yang, F. Chen, D. Zhang, H. Bian, Y. Ou, J. Si, G. Du and X. Hou, *Appl. Phys. A*, 2013, **111**, 243–249.
42 J. Yong, Q. Yang, F. Chen, G. Du, C. Shan, U. Farooq, J. Wang and X. Hou, *RSC Adv.*, 2015, **5**, 40907–40911.
43 M. Nosonovsky, *Langmuir*, 2007, **23**, 9919–9920.
44 C. Dorrer and J. Rühe, *Soft Matter*, 2009, **5**, 51–61.
45 B. Bhushan, K. Koch and Y. C. Jung, *Soft Matter*, 2008, **4**, 1799–1804.
46 D. Wu, S. Wu, Q. Chen, Y. Zhang, J. Yao, X. Yao, L. Niu, J. Wang, L. Jiang and H. Sun, *RSC Adv.*, 2011, **23**, 545–549.
47 J. Yong, Q. Yang, F. Chen, D. Zhang, U. Farooq, G. Du and X. Hou, *J. Mater. Chem. A*, 2014, **2**, 5499–5507.
48 S. Yang, J. Ju, Y. C. Qiu, Y. X. He, X. L. Wang, S. X. Dou, K. S. Liu and L. Jiang, *Small*, 2014, **10**, 294–299.
49 D. Wu, J. N. Wang, S. Z. Wu, Q. D. Chen, S. Zhao, H. Zhang, H. B. Sunvz and L. Jiang, *Adv. Funct. Mater.*, 2011, **21**, 2927–2932.